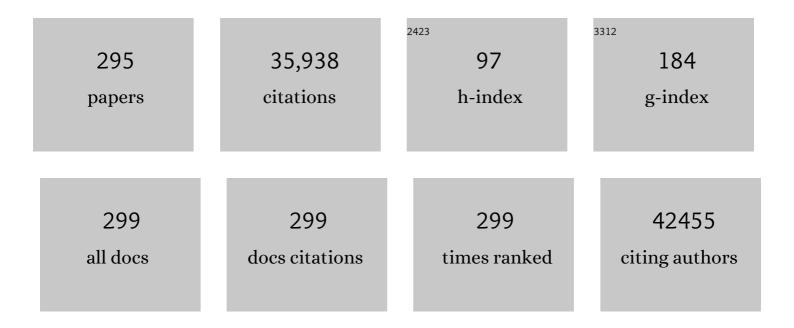


List of Publications by Year in descending order

Source: https://exaly.com/author-pdf/2448590/publications.pdf Version: 2024-02-01



TINC YU

#	Article	IF	CITATIONS
1	Carbonâ€Based Dots Coâ€doped with Nitrogen and Sulfur for High Quantum Yield and Excitationâ€Independent Emission. Angewandte Chemie - International Edition, 2013, 52, 7800-7804.	7.2	1,872
2	Uniaxial Strain on Graphene: Raman Spectroscopy Study and Band-Gap Opening. ACS Nano, 2008, 2, 2301-2305.	7.3	1,409
3	A library of atomically thin metal chalcogenides. Nature, 2018, 556, 355-359.	13.7	1,225
4	Raman spectroscopy and imaging of graphene. Nano Research, 2008, 1, 273-291.	5.8	1,181
5	Graphene Thickness Determination Using Reflection and Contrast Spectroscopy. Nano Letters, 2007, 7, 2758-2763.	4.5	1,034
6	αâ€Fe ₂ O ₃ Nanoflakes as an Anode Material for Liâ€Ion Batteries. Advanced Functional Materials, 2007, 17, 2792-2799.	7.8	1,024
7	Pyridinic N doped graphene: synthesis, electronic structure, and electrocatalytic property. Journal of Materials Chemistry, 2011, 21, 8038.	6.7	896
8	Raman Studies of Monolayer Graphene: The Substrate Effect. Journal of Physical Chemistry C, 2008, 112, 10637-10640.	1.5	663
9	Nitrogen and Sulfur Codoped Graphene: Multifunctional Electrode Materials for Highâ€₽erformance Liâ€Ion Batteries and Oxygen Reduction Reaction. Advanced Materials, 2014, 26, 6186-6192.	11.1	598
10	Mechanical Exfoliation and Characterization of Single―and Few‣ayer Nanosheets of WSe ₂ , TaS ₂ , and TaSe ₂ . Small, 2013, 9, 1974-1981.	5.2	544
11	Hysteresis of Electronic Transport in Graphene Transistors. ACS Nano, 2010, 4, 7221-7228.	7.3	526
12	Synthesis and Optical Properties of Largeâ€Area Singleâ€Crystalline 2D Semiconductor WS ₂ Monolayer from Chemical Vapor Deposition. Advanced Optical Materials, 2014, 2, 131-136.	3.6	513
13	The Origin of Fluorescence from Graphene Oxide. Scientific Reports, 2012, 2, 792.	1.6	505
14	Raman spectroscopy of epitaxial graphene on a SiC substrate. Physical Review B, 2008, 77, .	1.1	477
15	Strain and structure heterogeneity in MoS2 atomic layers grown by chemical vapour deposition. Nature Communications, 2014, 5, 5246.	5.8	453
16	Epitaxial Growth of Branched αâ€Fe ₂ O ₃ /SnO ₂ Nanoâ€Heterostructures with Improved Lithiumâ€Ion Battery Performance. Advanced Functional Materials, 2011, 21, 2439-2445.	7.8	439
17	Seed-assisted synthesis of highly ordered TiO2@α-Fe2O3 core/shell arrays on carbon textiles for lithium-ion battery applications. Energy and Environmental Science, 2012, 5, 6559.	15.6	421
18	Bioâ€Inspired Nacreâ€Iike Composite Films Based on Graphene with Superior Mechanical, Electrical, and Biocompatible Properties. Advanced Materials, 2012, 24, 3426-3431.	11.1	389

#	Article	IF	CITATIONS
19	Threeâ€Dimensional Co ₃ O ₄ @MnO ₂ Hierarchical Nanoneedle Arrays: Morphology Control and Electrochemical Energy Storage. Advanced Functional Materials, 2014, 24, 3815-3826.	7.8	378
20	Ordered Mesoporous Silicas and Carbons with Large Accessible Pores Templated from Amphiphilic Diblock Copolymer Poly(ethylene oxide)-b-polystyrene. Journal of the American Chemical Society, 2007, 129, 1690-1697.	6.6	377
21	Raman Spectroscopy Study of Lattice Vibration and Crystallographic Orientation of Monolayer MoS ₂ under Uniaxial Strain. Small, 2013, 9, 2857-2861.	5.2	363
22	Large-scale synthesis and field emission properties of vertically oriented CuO nanowire films. Nanotechnology, 2005, 16, 88-92.	1.3	348
23	Multifunctional CuO nanowire devices: p-type field effect transistors and CO gas sensors. Nanotechnology, 2009, 20, 085203.	1.3	323
24	Strain-induced direct–indirect bandgap transition and phonon modulation in monolayer WS2. Nano Research, 2015, 8, 2562-2572.	5.8	323
25	Thickness-Dependent Reversible Hydrogenation of Graphene Layers. ACS Nano, 2009, 3, 1781-1788.	7.3	320
26	Rationally Designed Hierarchical TiO ₂ @Fe ₂ O ₃ Hollow Nanostructures for Improved Lithium Ion Storage. Advanced Energy Materials, 2013, 3, 737-743.	10.2	296
27	High-quality monolayer superconductor NbSe2 grown by chemical vapour deposition. Nature Communications, 2017, 8, 394.	5.8	290
28	Observation of Excitonic Fine Structure in a 2D Transition-Metal Dichalcogenide Semiconductor. ACS Nano, 2015, 9, 647-655.	7.3	288
29	Nonblinking, Intense Two-Dimensional Light Emitter: Monolayer WS ₂ Triangles. ACS Nano, 2013, 7, 10985-10994.	7.3	281
30	Thermal conductivity determination of suspended mono- and bilayer WS2 by Raman spectroscopy. Nano Research, 2015, 8, 1210-1221.	5.8	280
31	Controllable Design of MoS ₂ Nanosheets Anchored on Nitrogenâ€Doped Graphene: Toward Fast Sodium Storage by Tunable Pseudocapacitance. Advanced Materials, 2018, 30, e1800658.	11.1	275
32	Evolution of disposable bamboo chopsticks into uniform carbon fibers: a smart strategy to fabricate sustainable anodes for Li-ion batteries. Energy and Environmental Science, 2014, 7, 2670-2679.	15.6	271
33	Optical Properties of 2D Semiconductor WS ₂ . Advanced Optical Materials, 2018, 6, 1700767.	3.6	265
34	Raman Mapping Investigation of Graphene on Transparent Flexible Substrate: The Strain Effect. Journal of Physical Chemistry C, 2008, 112, 12602-12605.	1.5	260
35	Two-dimensional carbon nanostructures: Fundamental properties, synthesis, characterization, and potential applications. Journal of Applied Physics, 2010, 108, .	1.1	258
36	Controlled Growth and Field-Emission Properties of Cobalt Oxide Nanowalls. Advanced Materials, 2005, 17, 1595-1599.	11,1	255

Ting Yu

#	Article	IF	CITATIONS
37	A general strategy toward graphene@metal oxide core–shell nanostructures for high-performance lithium storage. Energy and Environmental Science, 2011, 4, 4954.	15.6	255
38	Reduction of Fermi velocity in folded graphene observed by resonance Raman spectroscopy. Physical Review B, 2008, 77, .	1.1	247
39	Simple and rapid synthesis of ultrathin gold nanowires, their self-assembly and application in surface-enhanced Raman scattering. Chemical Communications, 2009, , 1984.	2.2	245
40	Chemically Driven Tunable Light Emission of Charged and Neutral Excitons in Monolayer WS ₂ . ACS Nano, 2014, 8, 11320-11329.	7.3	236
41	Valley depolarization due to intervalley and intravalley electron-hole exchange interactions in monolayer <mml:math xmlns:mml="http://www.w3.org/1998/Math/MathML"><mml:msub><mml:mtext>MoS</mml:mtext><mml:mn>2< Physical Review B, 2014, 89, .</mml:mn></mml:msub></mml:math>	/ <mark>1.1</mark> /mml:mn>	. <mark>232</mark> ≺/mml:msu
42	Edge chirality determination of graphene by Raman spectroscopy. Applied Physics Letters, 2008, 93, .	1.5	226
43	Symmetry Breaking of Graphene Monolayers by Molecular Decoration. Physical Review Letters, 2009, 102, 135501.	2.9	224
44	Multiwalled Carbon Nanotubes Beaded with ZnO Nanoparticles for Ultrafast Nonlinear Optical Switching. Advanced Materials, 2006, 18, 587-592.	11.1	219
45	Electronic structure of graphite oxide and thermally reduced graphite oxide. Carbon, 2011, 49, 1362-1366.	5.4	218
46	The effect of vacuum annealing on graphene. Journal of Raman Spectroscopy, 2010, 41, 479-483.	1.2	216
47	Fabrication of Co3O4-reduced graphene oxide scrolls for high-performance supercapacitor electrodes. Physical Chemistry Chemical Physics, 2011, 13, 14462.	1.3	215
48	Single CeO ₂ Nanowire Gas Sensor Supported with Pt Nanocrystals: Gas Sensitivity, Surface Bond States, and Chemical Mechanism. Journal of Physical Chemistry C, 2008, 112, 9061-9065.	1.5	212
49	Facile Synthesis of Hierarchically Porous Carbons from Dual Colloidal Crystal/Block Copolymer Template Approach. Chemistry of Materials, 2007, 19, 3271-3277.	3.2	207
50	Fabrication and SERS Performance of Silver-Nanoparticle-Decorated Si/ZnO Nanotrees in Ordered Arrays. ACS Applied Materials & Interfaces, 2010, 2, 1824-1828.	4.0	198
51	Probing Charged Impurities in Suspended Graphene Using Raman Spectroscopy. ACS Nano, 2009, 3, 569-574.	7.3	196
52	1T′ Transition Metal Telluride Atomic Layers for Plasmon-Free SERS at Femtomolar Levels. Journal of the American Chemical Society, 2018, 140, 8696-8704.	6.6	192
53	Investigation of individual CuO nanorods by polarized micro-Raman scattering. Journal of Crystal Growth, 2004, 268, 590-595.	0.7	191
54	Synergistic effect of hybrid carbon nantube–graphene oxide as a nanofiller in enhancing the mechanical properties of PVA composites. Journal of Materials Chemistry, 2011, 21, 10844.	6.7	191

#	Article	IF	CITATIONS
55	Carbon-decorated ZnO nanowire array: A novel platform for direct electrochemistry of enzymes and biosensing applications. Electrochemistry Communications, 2009, 11, 202-205.	2.3	189
56	Raman Characterization of ABA- and ABC-Stacked Trilayer Graphene. ACS Nano, 2011, 5, 8760-8768.	7.3	184
57	Enhanced Thermopower of Graphene Films with Oxygen Plasma Treatment. ACS Nano, 2011, 5, 2749-2755.	7.3	181
58	Electrically Tunable Valley-Light Emitting Diode (vLED) Based on CVD-Grown Monolayer WS ₂ . Nano Letters, 2016, 16, 1560-1567.	4.5	175
59	Electrocatalytic oxidation and reduction of H2O2 on vertically aligned Co3O4 nanowalls electrode: Toward H2O2 detection. Journal of Electroanalytical Chemistry, 2009, 625, 27-32.	1.9	173
60	Silane-catalysed fast growth of large single-crystalline graphene on hexagonal boron nitride. Nature Communications, 2015, 6, 6499.	5.8	173
61	NiFe2O4 nanoparticles formed in situ in silica matrix by mechanical activation. Journal of Applied Physics, 2002, 91, 6015-6020.	1.1	165
62	Strong correlation between ferromagnetism and oxygen deficiency in Cr-doped <mml:math xmlns:mml="http://www.w3.org/1998/Math/MathML" display="inline"><mml:mrow><mml:msub><mml:mrow><mml:mtext>In</mml:mtext></mml:mrow><mml:mn>2 Physical Review B, 2009, 79, .</mml:mn></mml:msub></mml:mrow></mml:math 	2 <b 111 2 <td>154 1></td>	154 1>
63	FeCl ₃ â€Based Fewâ€Layer Graphene Intercalation Compounds: Single Linear Dispersion Electronic Band Structure and Strong Charge Transfer Doping. Advanced Functional Materials, 2010, 20, 3504-3509.	7.8	154
64	Singleâ€Crystalline V ₂ O ₅ Ultralong Nanoribbon Waveguides. Advanced Materials, 2009, 21, 2436-2440.	11.1	146
65	Polarized Emission and Optical Waveguide in Crystalline Perylene Diimide Microwires. Advanced Materials, 2010, 22, 3661-3666.	11.1	146
66	3D Carbon/Cobaltâ€Nickel Mixedâ€Oxide Hybrid Nanostructured Arrays for Asymmetric Supercapacitors. Small, 2014, 10, 2937-2945.	5.2	146
67	Stacking-Dependent Optical Conductivity of Bilayer Graphene. ACS Nano, 2010, 4, 4074-4080.	7.3	145
68	The manipulation and assembly of CuO nanorods with line optical tweezers. Nanotechnology, 2004, 15, 1732-1736.	1.3	143
69	Second-Order Overtone and Combination Raman Modes of Graphene Layers in the Range of 1690â^'2150 cm ^{â^'1} . ACS Nano, 2011, 5, 1600-1605.	7.3	140
70	High-coercivity Co-ferrite thin films on (100)-SiO2 substrate. Applied Physics Letters, 2004, 84, 2596-2598.	1.5	135
71	Ordered Mesoporous Nanocrystalline Titanium arbide/Carbon Composites from In Situ Carbothermal Reduction. Advanced Materials, 2007, 19, 2301-2306.	11.1	135
72	Controlled synthesis of hierarchical graphene-wrapped TiO ₂ @Co ₃ O ₄ coaxial nanobelt arrays for high-performance lithium storage. Journal of Materials Chemistry A, 2013, 1, 273-281.	5.2	135

#	Article	IF	CITATIONS
73	Sensitivity enhanced biosensor using graphene-based one-dimensional photonic crystal. Sensors and Actuators B: Chemical, 2013, 182, 424-428.	4.0	133
74	Supramolecular Polymerization Promoted In Situ Fabrication of Nitrogenâ€Doped Porous Graphene Sheets as Anode Materials for Liâ€ion Batteries. Advanced Energy Materials, 2015, 5, 1500559.	10.2	133
75	Luminescence origin of carbon based dots obtained from citric acid and amino group-containing molecules. Carbon, 2017, 118, 319-326.	5.4	129
76	Dichroic spin–valley photocurrent in monolayer molybdenum disulphide. Nature Communications, 2015, 6, 7636.	5.8	128
77	Self-assembled graphene@PANI nanoworm composites with enhanced supercapacitor performance. RSC Advances, 2013, 3, 5851.	1.7	127
78	Room temperature ferromagnetism in partially hydrogenated epitaxial graphene. Applied Physics Letters, 2011, 98, .	1.5	126
79	Benzoxazole and benzimidazole heterocycle-grafted graphene for high-performance supercapacitor electrodes. Journal of Materials Chemistry, 2012, 22, 23439.	6.7	126
80	CNT/Ni hybrid nanostructured arrays: synthesis and application as high-performance electrode materials for pseudocapacitors. Energy and Environmental Science, 2011, 4, 5000.	15.6	125
81	Contrast and Raman spectroscopy study of single- and few-layered charge density wave material: 2H-TaSe2. Scientific Reports, 2013, 3, 2593.	1.6	120
82	Oriented graphene nanoribbons embedded in hexagonal boron nitride trenches. Nature Communications, 2017, 8, 14703.	5.8	119
83	Thickness-dependent patterning of MoS2 sheets with well-oriented triangular pits by heating in air. Nano Research, 2013, 6, 703-711.	5.8	118
84	<mml:math <br="" xmlns:mml="http://www.w3.org/1998/Math/MathML">display="inline"><mml:mi>G</mml:mi></mml:math> -band Raman double resonance in twisted bilayer graphene: Evidence of band splitting and folding. Physical Review B, 2009, 80, .	1,1	116
85	Cation migration and magnetic ordering in spinel CoFe2O4powder: micro-Raman scattering study. Journal of Physics Condensed Matter, 2002, 14, L613-L618.	0.7	110
86	Controlling the Growth Mechanism of ZnO Nanowires by Selecting Catalysts. Journal of Physical Chemistry C, 2007, 111, 17500-17505.	1.5	110
87	The study of interaction between graphene and metals by Raman spectroscopy. Journal of Applied Physics, 2011, 109, 07C501.	1.1	110
88	Catalyst-free pulsed-laser-deposited ZnO nanorods and their room-temperature photoluminescence properties. Applied Physics Letters, 2006, 88, 053110.	1.5	108
89	Room temperature nanocavity laser with interlayer excitons in 2D heterostructures. Science Advances, 2019, 5, eaav4506.	4.7	108
90	Comparison of surface-enhanced Raman scattering on graphene oxide, reduced graphene oxide and graphene surfaces. Carbon, 2013, 62, 422-429.	5.4	107

#	Article	IF	CITATIONS
91	Co-synthesis of ZnO–CuO Nanostructures by Directly Heating Brass in Air. Advanced Functional Materials, 2006, 16, 2415-2422.	7.8	104
92	Three dimensionals α-Fe2O3/polypyrrole (Ppy) nanoarray as anode for micro lithium ion batteries. Nano Energy, 2013, 2, 726-732.	8.2	102
93	Room-temperature 2D semiconductor activated vertical-cavity surface-emitting lasers. Nature Communications, 2017, 8, 543.	5.8	102
94	Thickness identification of two-dimensional materials by optical imaging. Nanotechnology, 2012, 23, 495713.	1.3	101
95	Pore Structures of Ordered Large Cage-Type Mesoporous Silica FDU-12s. Journal of Physical Chemistry B, 2006, 110, 21467-21472.	1.2	100
96	Fabrication of Graphene Nanodisk Arrays Using Nanosphere Lithography. Journal of Physical Chemistry C, 2009, 113, 6529-6532.	1.5	98
97	Hierarchical TiO2 nanobelts@MnO2 ultrathin nanoflakes core–shell array electrode materials for supercapacitors. RSC Advances, 2013, 3, 14413.	1.7	98
98	Excitation of surface electromagnetic waves in a graphene-based Bragg grating. Scientific Reports, 2012, 2, 737.	1.6	97
99	Reversible UV-Light-Induced Ultrahydrophobic-to-Ultrahydrophilic Transition in an α-Fe ₂ O ₃ Nanoflakes Film. Langmuir, 2008, 24, 10569-10571.	1.6	95
100	P -type electrical, photoconductive, and anomalous ferromagnetic properties of Cu2O nanowires. Applied Physics Letters, 2009, 94, .	1.5	95
101	Electronic Structures and Structural Evolution of Hydrogenated Graphene Probed by Raman Spectroscopy. Journal of Physical Chemistry C, 2011, 115, 1422-1427.	1.5	95
102	Influences of graphene oxide support on the electrochemical performances of graphene oxide-MnO2 nanocomposites. Nanoscale Research Letters, 2011, 6, 531.	3.1	95
103	Substrate-Friendly Synthesis of Metal Oxide Nanostructures Using a Hotplate. Small, 2006, 2, 80-84.	5.2	93
104	Orientation Controllable Growth of MoO ₃ Nanoflakes: Micro-Raman, Field Emission, and Birefringence Properties. Journal of Physical Chemistry C, 2009, 113, 20259-20263.	1.5	93
105	Crystallinity and surface effects on Young's modulus of CuO nanowires. Applied Physics Letters, 2007, 90, 163112.	1.5	92
106	InSe monolayer: synthesis, structure and ultra-high second-harmonic generation. 2D Materials, 2018, 5, 025019.	2.0	92
107	Thick wall mesoporous carbons with a large pore structure templated from a weakly hydrophobic PEO–PMMA diblock copolymer. Journal of Materials Chemistry, 2008, 18, 91-97.	6.7	91
108	Raman Study on the G Mode of Graphene for Determination of Edge Orientation. ACS Nano, 2010, 4, 3175-3180.	7.3	90

Ting Yu

#	Article	IF	CITATIONS
109	Largeâ€Scale Synthesis of Biâ€layer Graphene in Strongly Coupled Stacking Order. Advanced Functional Materials, 2011, 21, 911-917.	7.8	90
110	Toward High Energy Organic Cathodes for Liâ€ion Batteries: A Case Study of Vat Dye/Graphene Composites. Advanced Functional Materials, 2017, 27, 1603603.	7.8	90
111	Ferroelectric Transistors with Nanowire Channel: Toward Nonvolatile Memory Applications. ACS Nano, 2009, 3, 700-706.	7.3	89
112	Morphology Controllable Synthesis of α-Fe ₂ O ₃ 1D Nanostructures: Growth Mechanism and Nanodevice Based on Single Nanowire. Journal of Physical Chemistry C, 2008, 112, 10784-10788.	1.5	83
113	Progressively Exposing Active Facets of 2D Nanosheets toward Enhanced Pseudocapacitive Response and Highâ€Rate Sodium Storage. Advanced Materials, 2019, 31, e1900526.	11.1	83
114	Efficient field emission from α-Fe2O3 nanoflakes on an atomic force microscope tip. Applied Physics Letters, 2005, 87, 023103.	1.5	82
115	Modulating the electronic structures of graphene by controllable hydrogenation. Applied Physics Letters, 2010, 97, .	1.5	82
116	Gold on graphene as a substrate for surface enhanced Raman scattering study. Applied Physics Letters, 2010, 97, .	1.5	81
117	Vertically Aligned CuO Nanowires Based Electrode for Amperometric Detection of Hydrogen Peroxide. Electroanalysis, 2008, 20, 2153-2157.	1.5	80
118	Chemically engineered graphene oxide as high performance cathode materials for Li-ion batteries. Carbon, 2014, 76, 148-154.	5.4	80
119	Zone folding effect in Raman <mml:math <br="" xmlns:mml="http://www.w3.org/1998/Math/MathML">display="inline"><mml:mi>G</mml:mi></mml:math> -band intensity of twisted bilayer graphene. Physical Review B, 2012, 86, .	1.1	79
120	Size effect on the ferroelectric phase transition in SrBi2Ta2O9 nanoparticles. Journal of Applied Physics, 2003, 94, 618-620.	1.1	77
121	Enhanced ultra-low-frequency interlayer shear modes in folded graphene layers. Nature Communications, 2014, 5, 4709.	5.8	77
122	Microwave-assisted solvothermal preparation of nitrogen and sulfur co-doped reduced graphene oxide and graphene quantum dots hybrids for highly efficient oxygen reduction. Journal of Materials Chemistry A, 2014, 2, 20605-20611.	5.2	76
123	Controlled Synthesis of Atomically Thin 1T-TaS ₂ for Tunable Charge Density Wave Phase Transitions. Chemistry of Materials, 2016, 28, 7613-7618.	3.2	75
124	Mass Production of Largeâ€Sized, Nonlayered 2D Nanosheets: Their Directed Synthesis by a Rapid "Gelâ€Blowing―Strategy, and Applications in Li/Na Storage and Catalysis. Advanced Materials, 2018, 30, e1803569.	11.1	74
125	Terahertz Conductivity of Twisted Bilayer Graphene. Physical Review Letters, 2013, 110, 067401.	2.9	73
126	Facile fabrication of hierarchical ZnCo ₂ O ₄ /NiO core/shell nanowire arrays with improved lithium-ion battery performance. Nanoscale, 2014, 6, 6563-6568.	2.8	73

#	Article	IF	CITATIONS
127	Heterostructured TiO ₂ Spheres with Tunable Interiors and Shells toward Improved Packing Density and Pseudocapacitive Sodium Storage. Advanced Materials, 2019, 31, e1904589.	11.1	73
128	Nanostructure and Advanced Energy Storage: Elaborate Material Designs Lead to High-Rate Pseudocapacitive Ion Storage. ACS Nano, 2022, 16, 5131-5152.	7.3	73
129	Ultrathin single-crystal ZnO nanobelts: Ag-catalyzed growth and field emission property. Nanotechnology, 2010, 21, 255701.	1.3	72
130	Effects of CF4 plasma on the field emission properties of aligned multi-wall carbon nanotube films. Carbon, 2005, 43, 395-400.	5.4	71
131	Tunable wettability in surface-modified ZnO-based hierarchical nanostructures. Applied Physics Letters, 2008, 92, .	1.5	69
132	A Novel Graphene-Polysulfide Anode Material for High-Performance Lithium-Ion Batteries. Scientific Reports, 2013, 3, 2341.	1.6	68
133	Remarkable anisotropic phonon response in uniaxially strained few-layer black phosphorus. Nano Research, 2015, 8, 3944-3953.	5.8	68
134	Enhanced field emission from O2 and CF4 plasma-treated CuO nanowires. Chemical Physics Letters, 2006, 419, 458-463.	1.2	66
135	Size Selective Assembly of Colloidal Particles on a Template by Directed Self-Assembly Technique. Langmuir, 2006, 22, 8248-8252.	1.6	65
136	Ultrafast Electronâ^'Optical Phonon Scattering and Quasiparticle Lifetime in CVD-Grown Graphene. ACS Nano, 2011, 5, 3278-3283.	7.3	63
137	Engineering Valley Polarization of Monolayer WS ₂ : A Physical Doping Approach. Small, 2019, 15, e1805503.	5.2	62
138	Controlled growth of SnO2@Fe2O3 double-sided nanocombs as anodes for lithium-ion batteries. Nanoscale, 2012, 4, 4459.	2.8	60
139	Largeâ€Area Atomic Layers of the Chargeâ€Densityâ€Wave Conductor TiSe ₂ . Advanced Materials, 2018, 30, 1704382.	11.1	60
140	Photocontrolled Molecular Structural Transition and Doping in Graphene. ACS Nano, 2012, 6, 8878-8886.	7.3	58
141	Synthesis, characterization and opto-electrical properties of ternary Zn ₂ SnO ₄ nanowires. Nanotechnology, 2010, 21, 465706.	1.3	57
142	Femtosecond UV-pump/visible-probe measurements of carrier dynamics in stacked graphene films. Applied Physics Letters, 2010, 97, 163103.	1.5	56
143	Raman spectra of out-of-plane phonons in bilayer graphene. Physical Review B, 2011, 84, .	1.1	55
144	Formation of graphene oxide gel via the π-stacked supramolecular self-assembly. RSC Advances, 2012, 2, 12204.	1.7	55

Ting Yu

#	Article	IF	CITATIONS
145	The origin of sub-bands in the Raman D-band of graphene. Carbon, 2012, 50, 4252-4258.	5.4	54
146	Near-field Raman imaging using optically trapped dielectric microsphere. Optics Express, 2008, 16, 7976.	1.7	52
147	Fabrication of graphene nanogap with crystallographically matching edges and its electron emission properties. Applied Physics Letters, 2010, 96, .	1.5	52
148	Diffusion-controlled evolution of core–shell nanowire arrays into integrated hybrid nanotube arrays for Li-ion batteries. Nanoscale, 2013, 5, 8105.	2.8	52
149	Stacking sequence determines Raman intensities of observed interlayer shear modes in 2D layered materials – A general bond polarizability model. Scientific Reports, 2015, 5, 14565.	1.6	51
150	Light-Tunable 1T-TaS ₂ Charge-Density-Wave Oscillators. ACS Nano, 2018, 12, 11203-11210.	7.3	51
151	Facile synthesis and shape evolution of highly symmetric 26-facet polyhedral microcrystals of Cu2O. CrystEngComm, 2009, 11, 2291.	1.3	50
152	Electrical transport and photovoltaic effects of core–shell CuO/C60nanowire heterostructure. Nanotechnology, 2009, 20, 065203.	1.3	50
153	Effects of nanocrystal formation on the soft magnetic properties of Fe-based bulk metallic glasses. Applied Physics Letters, 2011, 99, .	1.5	50
154	Morphology-controlled synthesis and a comparative study of the physical properties of SnO2nanostructures: from ultrathin nanowires to ultrawide nanobelts. Nanotechnology, 2009, 20, 135605.	1.3	49
155	Raman spectroscopy of morphology-controlled deposition of Au on graphene. Carbon, 2013, 59, 487-494.	5.4	49
156	Molecular‣evel Design of Hierarchically Porous Carbons Codoped with Nitrogen and Phosphorus Capable of In Situ Selfâ€Activation for Sustainable Energy Systems. Small, 2017, 13, 1602010.	5.2	47
157	High-rate, long cycle-life Li-ion battery anodes enabled by ultrasmall tin-based nanoparticles encapsulation. Energy Storage Materials, 2018, 14, 169-178.	9.5	47
158	Localized suppression of longitudinal-optical-phonon–exciton coupling in bent ZnO nanowires. Nanotechnology, 2010, 21, 445706.	1.3	46
159	Tailoring Wettability Change on Aligned and Patterned Carbon Nanotube Films for Selective Assembly. Journal of Physical Chemistry B, 2007, 111, 1672-1678.	1.2	45
160	Engineering Morphologies of Cobalt Pyrophosphates Nanostructures toward Greatly Enhanced Electrocatalytic Performance of Oxygen Evolution Reaction. Small, 2018, 14, e1801068.	5.2	45
161	Inâ€Plane Anisotropic Thermal Conductivity of Fewâ€Layered Transition Metal Dichalcogenide Tdâ€WTe ₂ . Advanced Materials, 2019, 31, e1804979.	11.1	45
162	Ultra-sharp α-Fe2O3 nanoflakes: growth mechanism and field-emission. Applied Physics A: Materials Science and Processing, 2007, 89, 115-119.	1.1	44

#	Article	IF	CITATIONS
163	Potassium Tungsten Bronze Nanowires: Polarized Microâ€Raman Scattering of Individual Nanowires and Electron Field Emission from Nanowire Films. Advanced Materials, 2008, 20, 352-356.	11.1	44
164	Thickness-dependent azobenzene doping in mono- and few-layer graphene. Carbon, 2012, 50, 201-208.	5.4	44
165	Redox-crosslinked graphene networks with enhanced electrochemical capacitance. Journal of Materials Chemistry A, 2014, 2, 12924.	5.2	44
166	Resonant Raman spectroscopy of (Mn,Co)-codoped ZnO films. Journal of Applied Physics, 2008, 103, .	1.1	43
167	Visualization of arrangements of carbon atoms in graphene layers by Raman mapping and atomic-resolution TEM. Scientific Reports, 2013, 3, 1195.	1.6	43
168	Tipâ€enhanced Raman spectroscopy using singleâ€crystalline Ag nanowire as tip. Journal of Raman Spectroscopy, 2010, 41, 1156-1162.	1.2	42
169	Rapid and non-destructive identification of graphene oxide thickness using white light contrast spectroscopy. Carbon, 2013, 52, 528-534.	5.4	42
170	Seed-assisted synthesis of Co3O4@α-Fe2O3 core–shell nanoneedle arrays for lithium-ion battery anode with high capacity. RSC Advances, 2014, 4, 13241.	1.7	41
171	One-pot, aqueous-phase synthesis of graphene oxide functionalized with heterocyclic groups to give increased solubility in organic solvents. RSC Advances, 2013, 3, 45-49.	1.7	38
172	Enhancing and controlling valley magnetic response in MoS2/WS2 heterostructures by all-optical route. Nature Communications, 2019, 10, 4226.	5.8	38
173	Describing curved–planar π–π interactions: modeled by corannulene, pyrene and coronene. Physical Chemistry Chemical Physics, 2013, 15, 12694.	1.3	37
174	The transformation of a gold film on few-layer graphene to produce either hexagonal or triangular nanoparticles during annealing. Carbon, 2013, 52, 379-387.	5.4	37
175	Advanced nanobiomaterial strategies for the development of organized tissue engineering constructs. Nanomedicine, 2013, 8, 591-602.	1.7	37
176	Experimental evidences of topological surface states of β-Ag2Te. AIP Advances, 2013, 3, 032123.	0.6	36
177	Light Sources and Photodetectors Enabled by 2D Semiconductors. Small Methods, 2018, 2, 1800019.	4.6	35
178	Uniform Decoration of Reduced Graphene Oxide Sheets with Gold Nanoparticles. Journal of Nanotechnology, 2012, 2012, 1-8.	1.5	34
179	The characterization and application of p-type semiconducting mesoporous carbon nanofibers. Carbon, 2009, 47, 1841-1845.	5.4	31
180	Disorder-free sputtering method on graphene. AIP Advances, 2012, 2, .	0.6	31

#	Article	IF	CITATIONS
181	New Colloidal Lithographic Nanopatterns Fabricated by Combining Pre-Heating and Reactive Ion Etching. Nanoscale Research Letters, 2009, 4, 1324-1328.	3.1	30
182	Highly Ordered Monolayer, Multilayer, and Hybrid Films of Graphene Oxide Obtained by the Bubble Deposition Method. Journal of Physical Chemistry C, 2011, 115, 14678-14681.	1.5	30
183	A novel anti-cancer agent, acetyltanshinone IIA, inhibits oestrogen receptor positive breast cancer cell growth by down-regulating the oestrogen receptor. Cancer Letters, 2014, 346, 94-103.	3.2	30
184	Raman scattering investigation of twisted WS2/MoS2 heterostructures: interlayer mechanical coupling versus charge transfer. Nano Research, 2021, 14, 2215-2223.	5.8	29
185	Phase control of chromium oxide in selective microregions by laser annealing. Journal of Applied Physics, 2003, 93, 3951-3953.	1.1	28
186	Sequential Combination of Constituent Oxides in the Synthesis of Pb(Fe _{1/2} Nb _{1/2})O ₃ by Mechanical Activation. Journal of the American Ceramic Society, 2002, 85, 565-572.	1.9	28
187	Ultrafast carrier dynamics in pristine and FeCl3-intercalated bilayer graphene. Applied Physics Letters, 2010, 97, 141910.	1.5	28
188	Unveiling exceptionally robust valley contrast in AA- and AB-stacked bilayer WS ₂ . Nanoscale Horizons, 2019, 4, 396-403.	4.1	28
189	Evolution of Raman <mml:math xmlns:mml="http://www.w3.org/1998/Math/MathML"><mml:mi>G</mml:mi>and<mml:math xmlns:mml="http://www.w3.org/1998/Math/MathML"><mml:mi>G</mml:mi>G<mml:mo>â€2<td>:ma≯r/mu</td><td>nl:m257up></td></mml:mo></mml:math </mml:math 	:ma≯r/mu	nl:m257up>
190	folded graphene layers. Physical Review B, 2014, 89, . Room Temperature Commensurate Charge Density Wave on Epitaxially Grown Bilayer 2H-Tantalum Sulfide on Hexagonal Boron Nitride. ACS Nano, 2020, 14, 3917-3926.	7.3	27
191	Nitrogen-doped carbon-based dots prepared by dehydrating EDTA with hot sulfuric acid and their electrocatalysis for oxygen reduction reaction. RSC Advances, 2014, 4, 32791-32795.	1.7	26
192	Recognition of carbon nanotube chirality by phage display. RSC Advances, 2012, 2, 1466-1476.	1.7	25
193	How do the electron beam writing and metal deposition affect the properties of graphene during device fabrication?. Nanoscale, 2013, 5, 3352.	2.8	25
194	Patterning and fusion of CuO nanorods with a focused laser beam. Nanotechnology, 2005, 16, 1238-1244.	1.3	23
195	A new restriction effect of hard templates for the shrinkage of mesoporous polymer during carbonization. Chemical Communications, 2009, , 5033.	2.2	23
196	Long range surface plasmons in a symmetric graphene system with anisotropic dielectrics. Journal of Optics (United Kingdom), 2013, 15, 055002.	1.0	23
197	Visualizing the Anomalous Charge Density Wave States in Graphene/NbSe ₂ Heterostructures. Advanced Materials, 2020, 32, e2003746.	11.1	23
198	Revealing the interactions between pentagon–octagon–pentagon defect graphene and organic donor/acceptor molecules: a theoretical study. Physical Chemistry Chemical Physics, 2015, 17, 4919-4925.	1.3	22

#	Article	IF	CITATIONS
199	B-site disordering in Pb(Sc1/2Ta1/2)O3 by mechanical activation. Applied Physics Letters, 2003, 82, 4773-4775.	1.5	21
200	Encapsulation of nanoscale metal oxides into an ultra-thin Ni matrix for superior Li-ion batteries: a versatile strategy. Nanoscale, 2014, 6, 12990-13000.	2.8	21
201	Femtosecond pump–probe spectroscopy of graphene oxide in water. Journal Physics D: Applied Physics, 2014, 47, 094008.	1.3	21
202	Room-temperature continuous-wave vertical-cavity surface-emitting lasers based on 2D layered organic–inorganic hybrid perovskites. APL Materials, 2021, 9, 071106.	2.2	21
203	Enhanced Field Emission from Argon Plasma-Treated Ultra-sharp α-Fe2O3Nanoflakes. Nanoscale Research Letters, 2009, 4, 1115-1119.	3.1	20
204	Surface enhanced Raman scattering of aged graphene: Effects of annealing in vacuum. Applied Physics Letters, 2011, 99, .	1.5	20
205	Tunable excitonic emission of monolayer WS2 for the optical detection of DNA nucleobases. Nano Research, 2018, 11, 1744-1754.	5.8	20
206	Probing magnetic-proximity-effect enlarged valley splitting in monolayer WSe2 by photoluminescence. Nano Research, 2018, 11, 6252-6259.	5.8	20
207	Structural study of refractory-metal-free C40 TiSi2 and its transformation to C54 TiSi2. Applied Physics Letters, 2002, 80, 2266-2268.	1.5	19
208	Study of electromagnetic enhancement for surface enhanced Raman spectroscopy of SiC graphene. Applied Physics Letters, 2012, 100, 191601.	1.5	19
209	Long-range magnetic coupling across a polar insulating layer. Nature Communications, 2016, 7, 11015. Revealing electronic nature of broad bound exciton bands in two-dimensional semiconducting	5.8	19
210	<pre><mml:math xmlns:mml="http://www.w3.org/1998/Math/MathML"><mml:mrow><mml:mi mathvariant="normal">W</mml:mi><mml:msub><mml:mi mathvariant="normal">S</mml:mi><mml:mn>2</mml:mn></mml:msub></mml:mrow></mml:math> and <mml:math< pre=""></mml:math<></pre>	0.9	19
211	xmlns:mml="http://www.w3.org/1998/Math/MathML"> < mml:mrow> < mml:mi>Mo < mml:msub> < mml:m A novel approach to the construction of 3-D ordered macrostructures with polyhedral particles. Journal of Materials Chemistry, 2008, 18, 408-415.	i 6.7	18
212	Surfactant-assisted encapsulation of uniform SnO ₂ nanoparticles in graphene layers for high-performance Li-storage. 2D Materials, 2015, 2, 014005.	2.0	18
213	Direct observation of inner and outer G′ band double-resonance Raman scattering in free standing graphene. Applied Physics Letters, 2012, 100, .	1.5	17
214	Strong magnetophonon resonance induced triple G-mode splitting in graphene on graphite probed by micromagneto Raman spectroscopy. Physical Review B, 2013, 88, .	1.1	17
215	A Generic Micropatterning Platform to Direct Human Mesenchymal Stem Cells from Different Origins Towards Myogenic Differentiation. Macromolecular Bioscience, 2013, 13, 799-807.	2.1	17
216	Continuousâ€Wave Vertical Cavity Surfaceâ€Emitting Lasers based on Single Crystalline Lead Halide Perovskites. Advanced Optical Materials, 2021, 9, 2001982.	3.6	16

#	Article	IF	CITATIONS
217	Characterization of stearic acid adsorption on Ni(111) surface by experimental and first-principles study approach. Journal of Applied Physics, 2011, 109, 07C115.	1.1	15
218	Growth of horizontally aligned dense carbon nanotubes from trench sidewalls. Nanotechnology, 2011, 22, 265614.	1.3	15
219	Synthesis of Atomically Thin 1Tâ€TaSe ₂ with a Strongly Enhanced Chargeâ€Đensityâ€Wave Order. Advanced Functional Materials, 2020, 30, 2001903.	7.8	15
220	Effects of mechanical activation on the formation of PbTiO3 from amorphous Pb–Ti–O precursor. Journal of Applied Physics, 2003, 93, 3470-3474.	1.1	14
221	Bâ€5ite Order–Disorder Transition in Pb(Mg _{1/3} Nb _{2/3})O ₃ –Pb(Mg _{1/2} W _{1/2})O _{ Triggered by Mechanical Activation. Journal of the American Ceramic Society, 2002, 85, 833-838.}	3ĸ/sub>	14
222	Visualization and investigation of Si–C covalent bonding of single carbon nanotube grown on silicon substrate. Applied Physics Letters, 2008, 93, 103111.	1.5	14
223	High-temperature lasing characteristics of randomly assembled ZnO nanowires with a ridge waveguide. Journal of Applied Physics, 2009, 106, .	1.1	14
224	Recent nanosheet-based materials for monovalent and multivalent ions storage. Energy Storage Materials, 2020, 25, 382-403.	9.5	14
225	Salt effect on thermodynamics and kinetics of a single RNA base pair. Rna, 2020, 26, 470-480.	1.6	14
226	Ultrasensitive Photodetectors Promoted by Interfacial Charge Transfer from Layered Perovskites to Chemical Vapor Depositionâ€Grown MoS ₂ . Small, 2021, 17, e2102461.	5.2	14
227	Metal nanowires for transparent conductive electrodes in flexible chromatic devices: a review. Environmental Chemistry Letters, 2022, 20, 3005-3037.	8.3	14
228	Nanocrystalline PbTiO3 powders from an amorphous Pb–Ti–O precursor by mechanical activation. Materials Chemistry and Physics, 2002, 75, 216-219.	2.0	13
229	Selfâ€Limited Oxidation: A Route to Form Graphene Layers from Graphite by Oneâ€Step Heating. Small, 2010, 6, 2837-2841.	5.2	13
230	Highly dispersed Pt nanoparticles on hierarchical titania nanoflowers with {010} facets for gas sensing and photocatalysis. Journal of Materials Science, 2019, 54, 6826-6840.	1.7	12
231	Excitonic Lasers in Atomically Thin 2D Semiconductors. , 2020, 2, 1328-1342.		12
232	A broadband nearâ€infrared Sc ₁ _{â^'} <i>_x</i> (PO ₃) ₃ : <i>X</i> Cr ^{3+phosphor with enhanced thermal stability and quantum yield by Yb³⁺ codoping. Journal of the American Ceramic Society, 2022, 105, 3403-3417.}	^{>} 1.9	12
233	High coercivity Co-ferrite thin films on SiO2 (100) substrate. Journal of Magnetism and Magnetic Materials, 2004, 282, 211-215.	1.0	11
234	Confocal white light reflection imaging for characterization of metal nanostructures. Optics Communications, 2008, 281, 5360-5363.	1.0	10

#	Article	IF	CITATIONS
235	Effect of near-field coupling on far-field inelastic scattering imaging of gold nanoparticles. Nanotechnology, 2008, 19, 395705.	1.3	10
236	Comment on "Raman spectra of misoriented bilayer graphene― Physical Review B, 2009, 79, .	1.1	10
237	Pulsed laser deposition of ZnO honeycomb structures on metal catalyst prepatterned Si substrates. Journal Physics D: Applied Physics, 2009, 42, 065417.	1.3	10
238	Annealing temperature dependence of exchange bias in BiFeO3/CoFe bilayers. Journal of Applied Physics, 2012, 111, 07D908.	1.1	10
239	Probing near Dirac point electron-phonon interaction in graphene. Optical Materials Express, 2012, 2, 1713.	1.6	10
240	Femtosecond energy relaxation in suspended graphene: phonon-assisted spreading of quasiparticle distribution. Applied Physics B: Lasers and Optics, 2012, 107, 131-136.	1.1	10
241	Low temperature photoresponse of monolayer tungsten disulphide. APL Materials, 2014, 2, .	2.2	10
242	A 3D topological Dirac semimetal/MoO ₃ thin film heterojunction infrared photodetector with a current reversal phenomenon. Journal of Materials Chemistry C, 2020, 8, 16024-16031.	2.7	10
243	Facile Synthesis of Bi2MoO6 Nanosheets@Nitrogen and Sulfur Codoped Graphene Composites for Sodium-ion Batteries. Chemical Research in Chinese Universities, 2020, 36, 115-119.	1.3	10
244	Large-scale metal oxide nanostructures on template-patterned microbowls: A simple method for growth of hierarchical structures. Materials Letters, 2008, 62, 389-393.	1.3	9
245	Observation of lowâ€wavenumber outâ€ofâ€plane optical phonon in fewâ€layer graphene. Journal of Raman Spectroscopy, 2013, 44, 70-74.	1.2	9
246	Unveiling the origin of anomalous low-frequency Raman mode in CVD-grown monolayer WS2. Nano Research, 2021, 14, 4314-4320.	5.8	9
247	Magnetic polaron conduction above the Curie temperature in Fe-doped Pr0.75Sr0.25MnO3. Journal of Physics Condensed Matter, 2002, 14, L141-L147.	0.7	8
248	SpinÂphonon coupling in rod-shaped half-metallic CrO2ultrafine particles: a magnetic Raman scattering study. Journal of Physics Condensed Matter, 2003, 15, L213-L217.	0.7	8
249	Facile "Scratching―Method with Common Metal Objects To Generate Large-Scale Catalyst Patterns Used for Growth of Single-Walled Carbon Nanotubes. ACS Applied Materials & Interfaces, 2009, 1, 1873-1877.	4.0	8
250	Raman mapping probing of tip-induced anomalous polarization behavior in V2O5 waveguiding nanoribbons. Applied Physics Letters, 2010, 96, .	1.5	8
251	Effects of Ga addition on structural and magnetic properties of nanocomposite Nd-Fe-B-Ti-C thick ribbons. Journal of Applied Physics, 2012, 111, .	1.1	8
252	Magnetic oscillation of optical phonon in ABA- and ABC-stacked trilayer graphene. Physical Review B, 2015, 91, .	1.1	8

#	Article	IF	CITATIONS
253	Electrical field tuning of magneto-Raman scattering in monolayer graphene. Nano Research, 2015, 8, 1139-1147.	5.8	8
254	Magnetic Modes in Rare Earth Perovskites: A Magnetic-Field-Dependent Inelastic Light Scattering study. Scientific Reports, 2016, 6, 36859.	1.6	8
255	Intrinsic excitonic emission and valley Zeeman splitting in epitaxial MS2 (M = Mo and W) monolayers on hexagonal boron nitride. Nano Research, 2018, 11, 6227-6236.	5.8	8
256	Enhanced photoluminescence of WS2/WO3 heterostructural QDs. Journal of Alloys and Compounds, 2020, 834, 155066.	2.8	8
257	Observation of Strong Valley Magnetic Response in Monolayer Transition Metal Dichalcogenide Alloys of Mo _{0.5} W _{0.5} Se ₂ and Mo _{0.5} W _{0.5} Se ₂ /WS ₂ Heterostructures. ACS Nano, 2021. 15. 8397-8406.	7.3	8
258	The Thinnest Light Disk: Rewritable Data Storage and Encryption on WS ₂ Monolayers. Advanced Functional Materials, 2021, 31, 2103140.	7.8	7
259	Calcium-dependent conformational transition of calmodulin determined by Fourier transform infrared spectroscopy. International Journal of Biological Macromolecules, 2013, 56, 57-61.	3.6	6
260	Mechanical activation-induced B site order–disorder transition in perovskite Pb(Mg1/3Nb2/3)O3–Pb(Mg1/2W1/2)O3. Materials Chemistry and Physics, 2002, 75, 211-215.	2.0	5
261	Metal Hydroxide and Metal Oxide Nanostructures from Metal Corrosion. Journal of Nanoscience and Nanotechnology, 2009, 9, 1496-1500.	0.9	5
262	A Novel Xanthone fromGarcinia oligantha. Helvetica Chimica Acta, 2013, 96, 494-498.	1.0	5
263	Carrier density and light helicity dependence of photocurrent in mono- and bilayer graphene. Semiconductor Science and Technology, 2018, 33, 114008.	1.0	5
264	Spatial variations of valley splitting in monolayer transition metal dichalcogenide. InformaÄnÃ- Materiály, 2020, 2, 585-592.	8.5	5
265	Observation of Bragg polaritons in monolayer tungsten disulphide. Nano Research, 2022, 15, 1479-1485.	5.8	5
266	Monolayer tungsten disulfide in photonic environment: Angle-resolved weak and strong light-matter coupling. Nano Research, 2022, 15, 5619-5625.	5.8	5
267	Influence of organic layer thickness on structure, magnetic, and transport properties of Langmuir-Blodgett ttb-CuPc/CoFe. Applied Physics Letters, 2013, 102, 022401.	1.5	4
268	Synthesis of "Cactus" Top-Decorated Aligned Carbon Nanotubes and Their Third-Order Nonlinear Optical Properties. Journal of Nanoscience and Nanotechnology, 2006, 6, 990-995.	0.9	3
269	Magnetic Properties and Magnetic Domain Structures Evolution Modulated by CoFeB Layer in [Pd/Co]/CoFeB/MgO/CoFeB/[Co/Pd] Perpendicular MTJ Films. IEEE Transactions on Magnetics, 2012, 48, 2812-2815.	1.2	3
270	Directly Grown K _{0.33} WO ₃ Nanosheet Film Electrode for Fast Direct Electron Transfer of Protein. ChemElectroChem, 2014, 1, 463-470.	1.7	3

#	Article	IF	CITATIONS
271	Magneto-Optical Study of Defect Induced Sharp Photoluminescence in LaAlO3 and SrTiO3. Scientific Reports, 2016, 6, 33145.	1.6	3
272	Deterministic and Scalable Generation of Exciton Emitters in 2D Semiconductor Nanodisks. Advanced Optical Materials, 2022, 10, .	3.6	3
273	In situ strain electrical atomic force microscopy study on twoâ€dimensional ternary transition metal dichalcogenides. InformaÄnÃ-Materiály, 2022, 4, .	8.5	3
274	Unique Dielectric Behavior of 0.6Pb(Ni _{1/2} W _{1/2})O ₃ ·0.4PbTiO ₃ Derived from Mechanical Activation. Journal of the American Ceramic Society, 2003, 86, 791-794.	1.9	2
275	Ion Exchange Synthesis of Cobalt Ion Modified Titanate Nanoarray as an Electrocatalyst toward Efficient Hydrogen Evolution Reaction. ACS Applied Energy Materials, 2019, 2, 8946-8955.	2.5	2
276	Polarization-Dependent Purcell Enhancement on a Two-Dimensional h-BN/WS ₂ Light Emitter with a Dielectric Plasmonic Nanocavity. Nano Letters, 2022, 22, 1649-1655.	4.5	2
277	Whiteâ€Light Driven Resonant Emission from a Monolayer Semiconductor. Advanced Materials, 2022, , 2103527.	11.1	2
278	Mechanism of simultaneous formation of refractory-metal free C40 and C49â€,TiSi[sub 2] induced by Q-switched Nd:Yttrium–aluminum–garnet laser irradiation. Journal of Vacuum Science & Technology an Official Journal of the American Vacuum Society B, Microelectronics Processing and Phenomena, 2005, 23, 480.	1.6	1
279	Formation of α-Fe ₂ O ₃ Nanoflakes by Heating Fe in Air. Solid State Phenomena, 2007, 121-123, 45-48.	0.3	1
280	Effects of O ₂ and Ar Reactive Ion Etching on the Field Emission Properties of Aligned CuO Nanowire Films. Solid State Phenomena, 2007, 121-123, 793-796.	0.3	1
281	Pulsed-laser-induced nc-Si and nc-Si/SiOx core–shell structures on Si substrates. Journal of Materials Research, 2008, 23, 994-997.	1.2	1
282	Bound magnetic polarons induced ferromagnetism in transition-metal-doped oxide nanostructures. , 2010, , .		1
283	Fabrication of all-in-one multifunctional phage liquid crystalline fibers. RSC Advances, 2013, 3, 20437.	1.7	1
284	Raman Spectroscopy Study of Two-Dimensional Materials Under Strain. Springer Series in Materials Science, 2019, , 111-129.	0.4	1
285	Optical characterization of two-dimensional semiconductors. , 2020, , 135-166.		1
286	Localization of Laterally Confined Modes in a 2D Semiconductor Microcavity. ACS Nano, 2022, 16, 4940-4946.	7.3	1
287	High-resolution Raman imaging by optically tweezing a dielectric microsphere. Materials Research Society Symposia Proceedings, 2007, 1025, 1.	0.1	0
288	Random lasing from ZnO nanowires system. , 2009, , .		0

Random lasing from ZnO nanowires system. , 2009, , . 288

#	Article	IF	CITATIONS
289	Raman mapping probing of V <inf>2</inf> O <inf>5</inf> waveguiding nanoribbons. , 2010, , .		Ο
290	Stacking dependent optical properties of bilayer graphene. , 2010, , .		0
291	Chemically derived graphene as an effective substrate to detect fluorescence molecules. , 2011, , .		0
292	Pulsatile shear stress and high glucose concentrations induced reactive oxigen species production in endothelial cells. , 2011, , .		0
293	Application of a FRET-based caspase sensor for screening anti-apoptosis compounds in a culture-plate-based high throughput assay. , 2011, , .		0
294	Low Frequency Raman Scattering of Two-Dimensional Materials Beyond Graphene. Springer Series in Surface Sciences, 2018, , 195-206.	0.3	0
295	Near-Field Raman Imaging of Nanostructures and Devices. , 0, , 677-697.		0